

# Modeling charge separation in charged nanochannels for single-molecule electrometry

Jörg Enderlein,<sup>1, 2, a)</sup> Damir Sakhapov,<sup>1</sup> Ingo Gregor,<sup>1</sup> Matteo Croci,<sup>3</sup> and Narain Karedla<sup>4</sup>

<sup>1)</sup>*III. Institute of Physics – Biophysics, Georg August University, 37077 Göttingen, Germany.*

<sup>2)</sup>*Cluster of Excellence “Multiscale Bioimaging: from Molecular Machines to Networks of Excitable Cells” (MBExC), Georg August University, 37077 Göttingen, Germany.*

<sup>3)</sup>*Mathematical Institute, University of Oxford, Oxford, OX2 6GG, UK.*

<sup>4)</sup>*The Rosalind Franklin Institute, Harwell Campus, Didcot, OX11 0FA, UK.*

(Dated: August 11, 2022)

We model the transport of electrically charged solute molecules by a laminar flow within a nanoslit microfluidic channel with electrostatic surface potential. We derive the governing convection-diffusion equation, solve it numerically, and compare it with a Taylor-Aris-like approximation which gives excellent results for small Péclet numbers. We discuss our results in the light of designing an assay that can measure simultaneously the hydrodynamic size and electric charge of single molecules by tracking their motion in such nanoslit channels with electrostatic surface potential.

PACS numbers: 42.25.Fx, 42.50.Pq, 78.67.Bf

## I. INTRODUCTION

Structure and electrical charge are fundamental characteristics of biological molecules. Electrostatic effects are ubiquitous and dominate the activities and properties of many biomolecules. The main driving forces behind protein folding are the burying hydrophobic amino acid residues in the interior, the formation of salt bridges, and the formation of favorable energetic contacts of polar groups on the surface with solvent molecules. Ionic or ionizable groups on the surface of biomolecules play crucial roles in fundamental biological processes ranging from ligand recognition, signaling, protein folding, aggregation, enzymatic catalysis to redox reactions<sup>1–9</sup>. Metamorphic proteins and nucleic acid chains exhibit more than one folded active conformation in native conditions, often with different functions<sup>10–12</sup>. To investigate the structure-function relation of biomolecules, one requires knowledge of the full energy landscape and the effective charge on multiple pre-existing conformational isomers. Today, established techniques such as X-ray crystallography, small-angle X-ray scattering (SAXS), small-angle neutron scattering (SANS), magnetic resonance spectroscopy (NMR), and cryo-electron microscopy (cryoEM) are capable of delivering detailed atomic information on biomolecules (see for example<sup>13</sup>). As a result, theoretical structure-based electrostatic calculations are now routinely performed and used to dissect the structure-function inter-relationships and properties of these biomolecules. However, computational methods that perform structure-based electrostatic calculations face challenges when simulating specific biomolecule-ion interactions or biomolecule-biomolecule interactions in cellular settings where they are immersed in a solution of numerous ions and other small molecules and macromolecules. To handle important effects such as preferential hydration, ion-ion competition, charge regulation, or solvation is computationally expensive which severely limits the temporal and spatial scales

of these calculations, often leading to inaccurate results<sup>14</sup>. Although recent experimental advances are beginning to explore the energy landscapes of proteins and nucleic acid chains<sup>15,16</sup>, measuring electric charges of biological molecules in ion-containing buffer solutions at single molecule level is far from trivial<sup>17–20</sup>.

Solid-state nanopores have been used to characterize the charge and size of biomolecules and they offer great potential for scalable high-throughput rapid protein and nucleic-acid analysis. The core principle here is to measure the dwell times of ionic current blockage while molecules (proteins, nucleic acids) chain through the nanopores. However, this method is limited by the passage time of a single amino or nucleic acid, which is typically on the order of 10 ns to 1  $\mu$ s, poor signal-to-noise ratio due to thermal noise, interactions with the nanopore walls, and the detrimental effect of the applied high voltages on the protein or oligonucleotide structure itself<sup>21,22</sup>. Recently, a high-precision method to measure the electrical charge on single nanometer-scale objects using a geometry-induced electrostatic fluidic trap has been introduced<sup>23,24</sup>. The chief principle of this method is to modulate the spatial interaction potential of a charged object by introducing topographical indentations onto a sub-micrometer channel with like-charged walls, to then stably confine the particles in local interaction potential minima. By measuring the escape rates of fluorescently labeled biomolecules in such traps, which scales exponentially with the potential difference of having a particle inside or outside the trap, their effective electrical charges were back-calculated with  $< 1e$  precision. Although the method has promising potential, there are a few major limitations that impact its accuracy in determining the electrical charges. These are the determination of surface charge properties of the silica walls that remains poorly resolved to date<sup>25–28</sup>, and the required *a priori* knowledge of the molecules' hydrodynamic radii that necessitates independent measurements. Furthermore, the uncertainty of determining the charge is often defined and limited by the accuracy of the *in silico* numerical simulations of the entire experiment and by the accuracy of the complex fabrication process.

<sup>a)</sup>Corresponding author, email: jenderl@gwdg.de

In the present article, we propose a new method for determining *simultaneously* the size and the *effective* electrical charge of fluorescently labeled biomolecules in a nanochannel with thin conductive surfaces. The core idea is to measure the charge-dependent drift velocity and the dispersion of biomolecules under lateral pressure-driven parabolic laminar flow inside a nanochannel (or capillary) having a constant electrostatic surface potential. For sufficiently small Péclet numbers (ratio between characteristic diffusive and convective transport times), the broadening of the concentration peaks can be used for measuring molecular diffusion coefficients. This broadening is perfectly described by the theory developed by Taylor and Aris, who derived an expression for the apparent diffusion constant of the concentration spreading as a function of the actual solute's diffusion constant, the channel size, and the mean flow velocity<sup>29–32</sup>. In this work, we consider a similar problem, the convective-diffusive transport of a solute along a planar nanoslit channel, but with channel walls having non-zero surface potential and for charged solute molecules. The electrostatic interaction with the channel walls and the Debye layer around them alters the transversal distribution of the charged species across the channel. When a pressure difference is applied along the channel, the mean transport rate of molecules is modified significantly by these interactions in a charge-dependent manner. Although electrokinetic transport has been modeled extensively in the past<sup>33–35</sup>, very few theoretical works have targeted the convective-diffusive transport of charged solute in a nanochannel and are mostly limited to neutral solute particles<sup>36,37</sup>. Since Faxén derived the correction factor for the drag coefficients of particles close to an interface in the beginning of the 20<sup>th</sup> century<sup>38</sup>, low Reynolds number hydrodynamics and classical Navier-Stokes equation have been used to model the transport of particles within confinements of similar dimensions. Quite recently, this classical framework was successfully applied to find approximate analytical formulas for the effective charge, diffusion coefficients, and mobility of proteins through nanopores<sup>39</sup>. In the next section, we develop the general theory for this problem and describe our approach to numerically solve the corresponding convection-diffusion equation. In the third section, we derive a Taylor-Aris-like approximation for this problem. In the fourth section, we present numerical and approximate results for realistic parameters, highlighting the feasibility of a single-molecule assay for measuring electric charge and diffusion by tracking single molecules in channels with non-zero surface voltage.

## II. THEORETICAL FOUNDATION

We consider the convective-diffusive transport of a solute in a slit channel of finite length  $L$  and width  $h$  (boundaries  $y = \pm h/2$ ) with a stationary laminar flow along the channel's axis ( $x$ -axis). Both surfaces of the slit channel are kept at the same constant surface potential (voltage), and the solute molecules that are transported by convection and diffusion bear the electric charge  $q$ . For the sake of simplicity, we consider the case where the ratio of solute size to channel width

is small enough to ignore Faxén's correction factors for the drag coefficient, or of any electroviscous effects<sup>40</sup>. This assumption holds true for the majority of biomolecules of interest that are smaller than or equal to 10 nm in diameter inside a slit with a width in the order of 100 nm. In this case, the solute's flux density is given by

$$\mathbf{j} = -D\nabla c(\mathbf{r}, t) + \left[ u(y)\hat{\mathbf{e}}_x - \frac{q}{\gamma}\partial_y\psi(y)\hat{\mathbf{e}}_y \right] c(\mathbf{r}, t) \quad (1)$$

where  $c(\mathbf{r}, t)$  is the local concentration of the solute molecules at position  $\mathbf{r} = \{x, y\}$  and time  $t$ ,  $D$  is the diffusion coefficient,  $u(y)$  is the  $y$ -dependent flow speed along the  $x$ -direction,  $\psi(y)$  is the  $y$ -dependent electric potential, and  $\gamma = k_B T/D$  is the molecular friction coefficient. This leads to the following PDE for the solute transport

$$\partial_t c = -\mathbf{div} \mathbf{j} = D\Delta c + D\mu\partial_y(c\partial_y\psi) - u\partial_x c \quad (2)$$

where we have introduced the abbreviation

$$\mu = \frac{q}{k_B T}.$$

For a pressure-driven flow within a constant pressure gradient, the flow speed is found by solving the stationary Stokes equation<sup>41</sup>

$$\eta\partial_y^2 u = \partial_x p,$$

where  $\eta$  is the solution's viscosity, and  $\partial_x p < 0$  is a constant pressure gradient along  $x$ . With the no-slip boundary conditions  $u(y = \pm h/2) = 0$ , this equation has the analytic solution

$$u(y) = \frac{3}{2}\bar{u}\left(1 - \frac{4y^2}{h^2}\right),$$

where  $\bar{u} = -h^2\partial_x p/12\eta$  is the mean flow velocity. In case of a non-zero slip velocity  $u_0$  on the surface, this slip velocity has only to be added to the just found velocity profile. However, slipping should be important only for non-wetting liquids or nanostructured surfaces, but less for smooth water/glass or water/metal interfaces, channel widths of 100 nm, and low Reynolds numbers as considered in the present paper<sup>42,43</sup>.

The electric potential  $\psi$  shall obey the linearized Poisson-Boltzmann equation

$$\partial_y^2 \psi = \kappa^2 \psi,$$

where  $\kappa$  is the inverse Debye length of the solvent which is given by

$$\kappa = \sqrt{\frac{2 \cdot 10^3 N_A e^2 I}{\epsilon_0 \epsilon k_B T}},$$

with  $N_A$  being the Avogadro-Loschmidt constant,  $e$  the elementary charge,  $\epsilon$  and  $I$  the dielectric constant and ionic strength (in mol/l) of the solution, respectively, and  $\epsilon_0$  the vacuum dielectric constant. In all numerical simulations below, we use  $\epsilon = 80.1$  for water at room temperature (20 °C). With

the boundary conditions  $\psi(y = \pm h/2) = \zeta$ , where  $\zeta$  denotes the surface-potential, this equation has the analytic solution

$$\psi(y) = \zeta \frac{\cosh(\kappa y)}{\cosh(\kappa h/2)}.$$

We look for a solution  $c(\mathbf{r}, t)$  of eq. (2) for periodic boundary conditions along the  $x$ -direction, i.e.  $c(0, y, t) = c(L, y, t)$ , and no-flux conditions at the channel boundaries, i.e.

$$(\partial_y c + \mu c \partial_y \psi)_{y=\pm h/2} = e^{-\mu \psi} \partial_y (c e^{\mu \psi})_{y=\pm h/2} = 0.$$

The boundary conditions at  $x = 0$  and  $x = L$  can essentially be set arbitrarily since their effect is negligible sufficiently away from the boundaries, particularly when  $L \gg h$ . We will seek this solution in the form

$$c(\mathbf{r}, t) = \sum_{k=-K}^K \tilde{w}_k(y, t) \exp(iq_k x - q_k^2 D t),$$

so that the concentration  $c(\mathbf{r}, t)$  is represented by a discrete Fourier series in the coordinate  $x$  with discrete Fourier frequencies  $q_k = 2\pi k/L$ , where  $2K + 1$  is the number of summed frequency components. Here, we have introduced new functions  $\tilde{w}_k(y, t)$  that depend only on the transverse coordinate  $y$  and time  $t$ . This automatically assures periodic boundary conditions along  $x$ . By inserting this *Ansatz* into eq. (2), one finds that the auxiliary functions  $\tilde{w}_k$  obey the elliptic partial differential equations

$$\partial_t \tilde{w}_k = D \partial_y^2 \tilde{w}_k + D \mu \partial_y (\tilde{w}_k \partial_y \psi) - i q_k u \tilde{w}_k \quad (3)$$

with initial values

$$\tilde{w}_{k,0}(y) = \frac{1}{L} \int_0^L dx \exp(-i q_k x) c_0(\mathbf{r}),$$

where  $c_0(\mathbf{r})$  is the initial concentration distribution at time  $t = 0$ . When introducing new variables

$$\tilde{\omega}_k = \tilde{w}_k \exp\left(\frac{\mu \psi}{2}\right)$$

eqs. (3) can be rewritten as

$$\partial_t \tilde{\omega}_k = D \partial_y^2 \tilde{\omega}_k - V_k(y) \tilde{\omega}_k, \quad (4)$$

with  $k$ -dependent complex-valued potentials

$$V_k(y) = i q_k u + D e^{\mu \psi/2} \partial_y^2 \left( e^{-\mu \psi/2} \right)$$

and boundary condition

$$\frac{\partial}{\partial y} \left[ \tilde{\omega}_k \exp\left(\frac{\mu \psi}{2}\right) \right]_{y=\pm h/2} = 0.$$

The eqs. (4) are much more amenable for numerical solution than the original PDEs, because they do not involve first-order derivatives in the coordinates (no convection terms). They can be solved in a standard way via discretization and solving the resulting algebraic equations, for details see ref.<sup>44,45</sup>.

### III. TAYLOR-ARIS APPROXIMATION

For convection-diffusion transport of solutes in flows within microfluidic channels, Taylor and Aris developed their famous approximation<sup>30,31,46</sup> which gives an excellent description of the actual situation for small Péclet numbers. One can extend this approximation to the case of convection-diffusion transport of electrically charged solutes in an electric field that is considered here. For this purpose, we expand the concentration  $c(x, y, t)$  into the form  $\exp(-\mu \psi) [\bar{a}(x, t) + b(x, y, t)]$ , where  $\bar{a}(x, t)$  does not depend on  $y$ ,  $b(x, y, t)$  describes small deviations from  $\bar{a}$ , and the factor  $\exp(-\mu \psi)$  is proportional to the Boltzmann equilibrium distribution of charge  $q$  in an electric potential  $\psi(y)$ . Inserting this into eq. (2) and integrating over the transversal coordinate  $y$  results in

$$\frac{\partial \bar{a}}{\partial t} = D \partial_x^2 \bar{a} - \langle u \rangle_\psi \partial_x \bar{a} - \langle u \partial_x b \rangle_\psi. \quad (5)$$

where the angular brackets denote the weighted average

$$\langle f \rangle_\psi = \frac{\int_{-h/2}^{h/2} dy e^{-\mu \psi} f(y)}{\int_{-h/2}^{h/2} dy e^{-\mu \psi}}.$$

Subtracting eq. (5) from eq. (2) leads to

$$\begin{aligned} \frac{\partial b}{\partial t} = & D (\partial_x^2 b + e^{\mu \psi} \partial_y e^{-\mu \psi} \partial_y b) \\ & - \delta u \partial_x \bar{a} - u \partial_x b + \langle u \partial_x b \rangle_\psi, \end{aligned}$$

where  $\delta u = u - \langle u \rangle_\psi$ . Following the arguments of Taylor and Aris<sup>30,31,46</sup> and assuming that the gradients of  $b$  along  $y$  are much bigger than gradients along  $x$ , and that the temporal change of  $b$  is negligible, the last equation can be approximately written as

$$D \partial_y e^{-\mu \psi} \partial_y b = e^{-\mu \psi} \delta u \partial_x \bar{a}.$$

Integration of this equation yields

$$\begin{aligned} b = & \frac{\partial_x \bar{a}}{D} \int_{-h/2}^y dy' e^{\mu \psi} \int_{-h/2}^{y'} dy'' e^{-\mu \psi} \delta u \\ & + A y e^{\mu \psi} - \frac{\partial_x \bar{a}}{D} B, \end{aligned} \quad (6)$$

with integration constants  $A$  and  $B$ . Constant  $A$  has to be zero to fulfill the boundary conditions, and constant  $B$  is determined by requiring that  $\langle b \rangle_\psi = 0$ , so that we find

$$B = \left\langle \int_{-h/2}^y dy' e^{\mu \psi} \int_{-h/2}^{y'} dy'' e^{-\mu \psi} \delta u \right\rangle_\psi.$$

Now, we can use this solution to calculate  $\langle u \partial_x b \rangle_\psi$  in eq. (5) which then leads to a partial differential equation for  $\bar{a}$  alone. Because the solution for  $b$  from eq. (6) is proportional to  $\partial_x \bar{a}$ , the resulting equation for  $\bar{a}$  is a convection-diffusion equation along only one spatial dimension  $x$  with drift velocity

$$u_{\text{drift}} = \langle u \rangle_\psi \quad (7)$$

and effective diffusion coefficient

$$D_{\text{eff}} = D + \frac{Bu_{\text{drift}}}{D} - \frac{1}{D} \left\langle u \int_{-h/2}^y dy' e^{\mu\psi} \int_{-h/2}^{y'} dy'' e^{-\mu\psi} \delta u \right\rangle_{\psi}. \quad (8)$$

In the case of zero electric field (or zero electric charge of solute) one finds  $u_{\text{drift}} = \bar{u}$  and

$$D_{\text{eff}} = D \left( 1 + \frac{h^2 \bar{u}^2}{210D^2} \right) = D \left( 1 + \frac{\text{Pe}^2}{210} \right),$$

in agreement with ref.<sup>47</sup>. In the last equation, Pe is the Péclet number,  $\text{Pe} = h\bar{u}/D$ .

For an initial solute concentration distribution of

$$c_0(x, y) = \frac{1}{\sqrt{2\pi\sigma_0^2}} \exp \left[ -\frac{(x-x_0)^2}{2\sigma_0^2} - \mu\psi(y) \right]$$

i.e. for a product of a Gaussian distribution with width  $\sigma_0$  along the  $x$ -direction and a Boltzmann equilibrium distribution along the  $y$ -direction, the approximate concentration distribution at time  $t$  is

$$c(x, y, t) = \frac{1}{\sqrt{2\pi\sigma^2(t)}} \exp \left\{ -\frac{[x - \bar{x}(t)]^2}{2\sigma^2(t)} - \mu\psi \right\} \quad (9)$$

with  $\bar{x}(t) = x_0 + u_{\text{drift}}t$  and  $\sigma^2(t) = \sigma_0^2 + 2D_{\text{eff}}t$ . Note that even in the presence of slip boundary conditions, eqs. (7) and (8) still represent the drift velocity and the effective diffusion coefficient, respectively. The mean flow velocity in this case is given by  $\bar{u} = -h^2 \partial_x p / 12\eta + u_0$ , where  $u_0$  is the fluid velocity at the boundaries.

#### IV. NUMERICAL RESULTS AND DISCUSSION

We numerically simulated the transport of a spatially localized concentration of solute along a 1 mm long slit channel with width  $h = 200$  nm and with surface potential of  $\zeta = 1$  V. The initial concentration distribution was assumed to be Gaussian along the  $x$ -direction with a spatial square-root variance  $\sigma_0 = 10$   $\mu\text{m}$ . We performed the numerical simulation for two scenarios: one with an electrically neutral solute, and one with a solute having an electric charge of  $q = 1e$ . The discretization grid of the numerical calculation had a grid spacing of 250 nm along the  $x$ -direction, and of 1 nm along the  $y$ -direction. The mean flow velocity was set to  $\bar{u} = 66.67$   $\mu\text{m}/\text{s}$ , and the solute's diffusion coefficient was assumed to be  $D = 100$   $\mu\text{m}^2/\text{s}$ . The calculational result is shown in Fig. 1, where the panels in the left column show the transport for electrically neutral molecules (i.e. for  $q = 0$ ), and the right panels for solute molecules with a single positive elementary charge. As can be seen, the electric field forces the charged molecules towards the center of the channel, which leads to an on average faster transport along the  $x$ -direction for the charged solute as compared to that of the neutral solute.

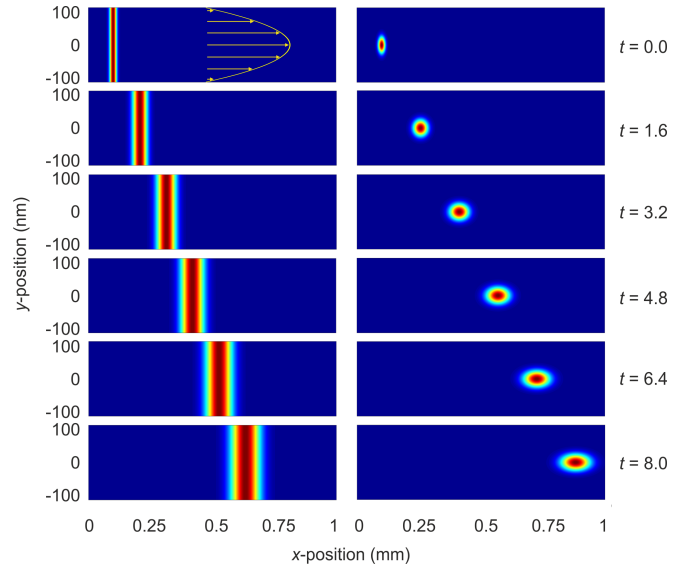


Figure 1. Numerical modeling of convection-diffusion in a slit channel of 200 nm width with pressure-driven flow for neutral (left column) and charged ( $q = 1e$ ) molecules (right column) using equation (4). The model parameters are: mean convection velocity  $\bar{u} = 66.67$   $\mu\text{m}/\text{s}$ , diffusion coefficient  $D = 100$   $\mu\text{m}^2/\text{s}$ , surface potential  $\zeta = 1$  V, Debye length of  $\kappa^{-1} = 45$  nm. The parabolic flow profile is sketched in the top left panel. Time values on the right are given in seconds.

A comparison of this exact numerical calculation with the Taylor-Aris approximation of eq. (9) shows that the approximation is virtually indistinguishable from the exact result, see Fig. 2, where a cross-section averaged broadening of concentrations at various  $x$ -positions are plotted for comparison. This is due to the extremely small Péclet number of  $\sim 0.018$  which is dominated by the small channel width  $h$ . For all parameter values relevant for the present study (average flow speed, channels size, viscosity), one remains always in the regime of small Péclet numbers, so that the Taylor-Aris approach is a perfect approximation of the exact results, but offering a tremendously better computational efficiency of more than five orders of magnitude (for example, the numerical computation time for Fig. 2 was  $\sim 450$  s, whereas the computation time for the Taylor-Aris approximation was  $\sim 3$  ms, using the same PC hardware and Matlab software platform). The Taylor-Aris approximation also clearly shows that the small Péclet numbers lead to an effective diffusion coefficient  $D_{\text{eff}}$  that is virtually equal to  $D$ . However, the drift velocity  $u_{\text{drift}}$  becomes strongly charge-dependent and differs considerably from  $\bar{u}$  for charged solute molecules, in stark contrast to classical Taylor-Aris dispersion which leads to an enhanced diffusion coefficient but unchanged drift velocity.

Using eq. (7), we calculated the dependence of the drift velocity as a function of surface potential  $\zeta$  and Debye length  $\kappa^{-1}$  (i.e. ionic strength  $I$ ) as shown in Fig. 3. The yellow line in Fig. 3 depicts the line of maximum drift velocity as a function of surface potential. For large surface potential above  $\zeta = 0.5$  V, this maximum drift velocity saturates and comes close to its maximally possible value of  $3\bar{u}/2$  (the maximum

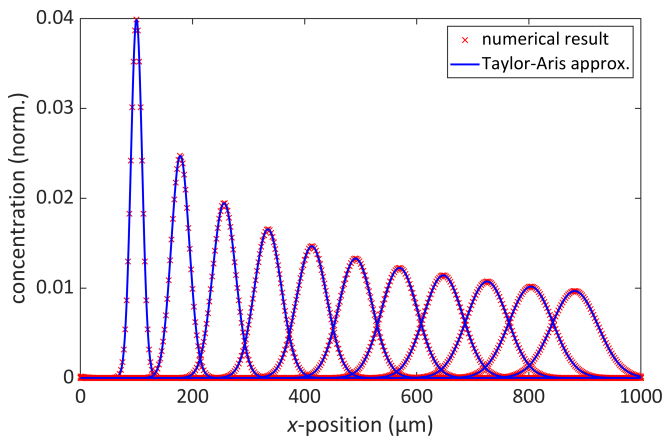


Figure 2. Comparison between numerical calculation shown in the right panels of Fig. 1 and the corresponding Taylor-Aris approximation of eq. (9). Shown is the temporal evolution of the cross-section averaged concentration as function of  $x$ -position.

flow velocity at the channel's center line). For negative surface potential, one sees a retardation of the drift velocity which is due to increasing concentration of solute close to the channel walls due to electrostatic attraction. Thus, convection-diffusion of solutes in the slit channel with sufficiently large surface potential will lead to a separation between neutral and charged solutes. However, for large surface potential values as on the right side of the figure, increasing the charge will nearly not change the drift velocity anymore. If one is interested in efficiently separating differently charged solutes, one should work with surface potentials where the slope of the yellow line in Fig. 2 is largest, i.e. close to  $\zeta \sim 0$ , but not too small so that one can observe efficient separation of different solutes within reasonable channel length (and time). If one aims for a drift velocity enhancement of  $\sim 10\%$  over  $\bar{u}$  for a

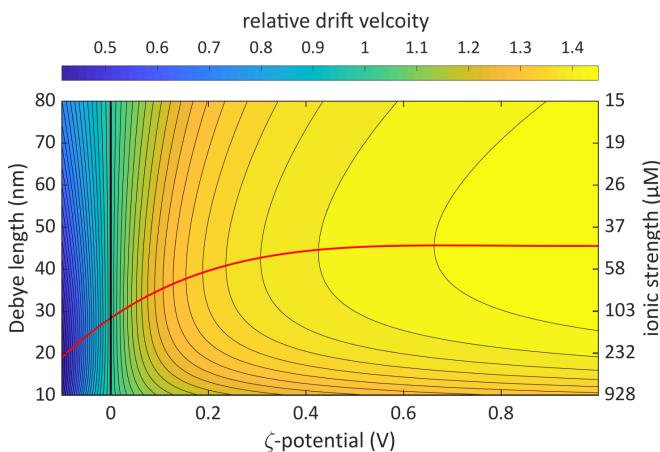


Figure 3. Relative drift velocity  $u_{\text{drift}}/\bar{u}$  as a function of surface potential (surface voltage) and Debye length (ionic strength). The yellow line is the line of maximum drift velocity as a function of surface potential. Calculations were done for the same channel and solute parameters as used for the right panels of Fig. 1.

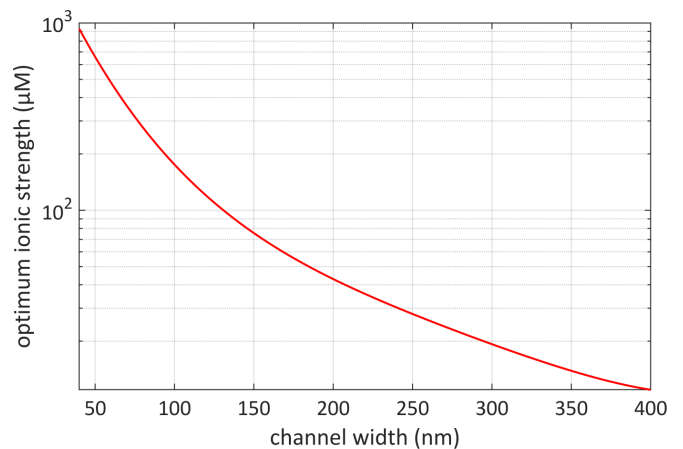


Figure 4. Ionic strength that maximizes drift velocity  $u_{\text{drift}}$  at  $\zeta = 1$  V surface potential as a function of channel width  $h$ . In Fig. 3, this value corresponds to the intersection of the yellow line with the right abscissa.

singly charged solute, reasonable surface potential values are around  $\zeta = 50$  mV for an ionic strength of ca.  $100 \mu\text{M}$  (channel width  $200$  nm). As can be seen from Fig. 3, working at even higher ionic strength is possible when correspondingly working at larger values of surface potential (see stretching of relative drift velocity values along horizontal axis for small Debye length i.e. high ionic strength). To estimate how the plot of Fig. 3 will change with smaller channel width, we calculated the ionic strength that maximizes the relative drift velocity at  $\zeta = 1$  V surface potential as a function of channel width. The result is shown in Fig. 4. As can be seen, for technically reasonable channel width values between  $40$  nm and  $400$  nm, this ionic strength varies between  $1 \mu\text{M}$  and  $1 \text{mM}$ , and this roughly gives an estimate how the vertical axes in Fig. 3 re-scales when changing the channel width. For example, when working with a channel having a width of  $40$  nm instead of  $200$  nm, one can work at ca.  $25$  times higher ionic strength while observing a similar behavior as shown in Fig. 3.

Finally, we would like to make some rough estimates for using drift velocity measurements in nanoslit microfluidic channels for charge determination of *single solute molecules*. For this purpose, we calculated, in the Taylor-Aris approximation of eq. (9), the relative drift velocity as a function of the product of electric charge and surface potential (please note that only this product determines the drift velocity, not the separate values of charge or surface potential). The result for a  $200$  nm wide channel at ca.  $100 \mu\text{M}$  ionic strength is presented in Fig. 5. The annotations in this figure refer to six different relative drift velocities for a solute molecule with a charge between  $1$  and  $6$  elementary charges at a surface potential of  $50$  mV. Let us denote by  $R$  the difference of relative drift velocities between two charge states differing by one elementary charge, and let us assume that one tracks the motion of a molecule along a channel of length  $L$ , then the mean difference in traveled distances after run length  $L$  is  $RL$ , while at the same time the diffusion-induced spreading of position is  $\sqrt{2DL/\bar{u}}$ . If we assume that for distinguishing different

charge states based on mean drift velocity, the mean difference in traveled distances should be at least three times bigger than the diffusion-induced spreading, then we find the following estimate for the required minimum run length (channel length  $L$ ) over which one has to track a molecule:

$$L = \frac{18D}{\bar{u}R^2} \quad (10)$$

Assuming a typical diffusion coefficient of  $100 \mu\text{m}^2/\text{s}$  (hydrodynamic radius of solute molecule ca. 1 nm) and a mean flow speed  $\bar{u}$  of  $1000 \mu\text{m}/\text{s}$ , then one needs a microfluidic channel length of ca.  $4500 \mu\text{m}$  for distinguishing between  $q = 5e$  and  $q = 6e$  ( $R \approx 0.02$ , see Fig. 5), with mean travel times (total observation time per molecule) of 3-4.5 s. To prevent photobleaching during such a long time, stroboscopic excitation could be employed. For smaller values of charges ( $q = 4e$  and  $q = 5e$ ,  $q = 3e$  and  $q = 4e$  etc.), shorter channel lengths would be sufficient. For example, one would need only a  $60 \mu\text{m}$  long channel for distinguishing between zero and one elementary charge ( $R \approx 0.17$ ), with a mean travel time of 40-60 ms, which would require, however, imaging at 1000 frames per second. But our estimate shows that by tracking molecules along sufficiently long nanoslit channels, one should be able to resolve between 0 and 6 charge states when using a microfluidic chip with a total channel length of 4.5 mm, which could be realized in a compact way by a meandering channel design. By comparing the absolute mean drift velocity  $u_{\text{drift}}$  with the mean flow velocity  $\bar{u}$  for an applied surface potential and given geometry of the slit, the absolute charge of the solute species can be estimated. Moreover, evaluation of a molecule's diffusive motion around its mean drift position would simultaneously allow for determining its diffusion coefficient and thus hydrodynamic size. This can be done using existing single particle tracking algorithms that employ a stochastic drift-diffusion model for the particle motion along the  $x$ -axis<sup>48,49</sup>. Note that in the presence of slip boundary conditions, the relative drift velocities  $R$  will decrease with increasing fluid velocity at the boundary, so that the minimum run length  $L$  required for distinguishing different charge states will be longer.

We would like to emphasize that the mean-field based theoretical approach presented here is applicable as long as the channel surfaces can be considered to be in the "far-field" of the charged molecules, i.e. at least one Debye length,  $\kappa^{-1}$ , away. The channel width and electrolyte concentration considered in this work satisfy this criterion, as shown in Fig. 4. Furthermore, the considered Debye lengths are substantially longer than the Bjerrum length (0.71 nm for water at room temperature), so that ion-ion correlations are not significant and the Poisson-Boltzmann theory remains generally valid<sup>50</sup>. The surface potential values that we consider in our paper and which are required for successfully separating charges are so large that the probability to find a (likely) charged molecule close to the walls is negligible as compared to the probability to find it towards the middle of the channel.

Importantly, the interaction of charged molecules with the channel walls is governed by their *effective* and not their formal structural charge. Whereas the latter can be derived from the structure of the molecular species in a straight-

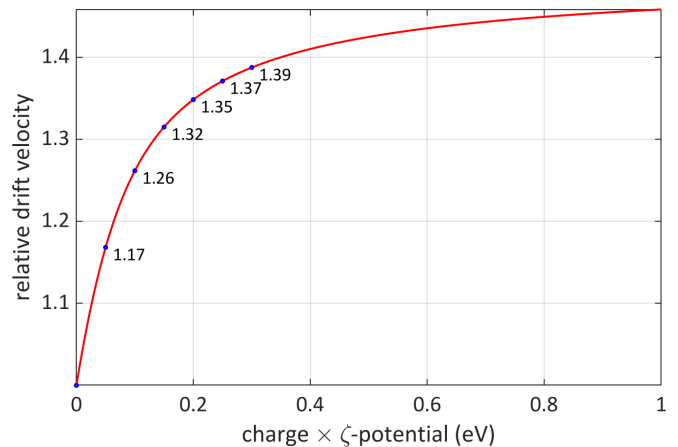


Figure 5. Relative drift velocity  $R = u_{\text{drift}}/\bar{u}$  as a function of the product of charge and surface potential for a channel width of 200 nm and a Debye length of 30 nm. The annotated five values are the relative drift velocities for solute molecules with 1 to 6 elementary charges at a surface potential of 50 mV on the channel walls.

forward manner, the former is a resultant of charge regulation and renormalization phenomena that take into account the acid-base equilibrium of the molecules' ionizable groups modified by their local environment and by intramolecular Coulomb interactions, as well as counter-ion condensation on the molecules' surface<sup>51</sup>. The free energy of the long-range interactions between a molecule and the channel walls at a given electrolyte concentration is determined by this effective charge<sup>52</sup>.

Finally, let us mention that a well-defined surface potential on the channel walls can be generated with transparent electrodes on these walls.

## V. CONCLUSION

We have considered the problem of the convection-diffusion of charged solute molecules in a nanoslit microfluidic channel with electric surface potential and transported by a laminar parabolic flow. We have derived the governing equations for this problem, and solved them numerically. We have also found a Taylor-Aris-like approximation of the solution which yields excellent results for small Péclet numbers. Finally, we have discussed our numerical results in the light of designing a single-molecule assay that could simultaneously measure hydrodynamics size and electric charge of biomolecules, providing reasonable estimates for channel width, length, surface potential and flow speed, and for the range of ionic strength values of the solvent for which such an assay could work. With our mean-field Poisson-Boltzmann theory, we currently consider only monovalent electrolytes neglecting ion-ion correlations, ion-specific effects such as ion affinity, and the finite size of ions. A suitable modified Poisson-Boltzmann equation can be incorporated in future that takes into account most of these effects.

## VI. DATA AVAILABILITY STATEMENT

No data were generated for this paper.

## VII. ACKNOWLEDGMENTS

JE acknowledges financing by the Deutsche Forschungsgemeinschaft (DFG, German Research Foundation) under Germany's Excellence Strategy - EXC 2067/1 - 390729940, and financing by the European Research Council (ERC) via project "smMIET" (Grant agreement No. 884488) under the European Union's Horizon 2020 research and innovation programme. MC would like to acknowledge the ICONIC EPSRC Programme Grant (EP/P020720/1) for support. NK acknowledges EPSRC funding for RFI.

## REFERENCES

- <sup>1</sup>MF Perutz. Electrostatic effects in proteins. *Science*, 201(4362):1187–1191, 1978.
- <sup>2</sup>James B Matthew. Electrostatic effects in proteins. *Annual review of biophysics and biophysical chemistry*, 14(1):387–417, 1985.
- <sup>3</sup>Raghavan Varadarajan, Thomas E Zewert, Harry B Gray, and Steven G Boxer. Effects of buried ionizable amino acids on the reduction potential of recombinant myoglobin. *Science*, 243(4887):69–72, 1989.
- <sup>4</sup>Hartmut Luecke, Hans-Thomas Richter, and Janos K Lanyi. Proton transfer pathways in bacteriorhodopsin at 2.3 angstrom resolution. *Science*, 280(5371):1934–1937, 1998.
- <sup>5</sup>Kim A. Sharp and Barry Honig. Electrostatic interactions in macromolecules: Theory and applications. *Annual Review of Biophysics and Biophysical Chemistry*, 19(1):301–332, 1990.
- <sup>6</sup>David Andelman. Introduction to electrostatics in soft and biological matter. In W Poon and D Andelman, editors, *Soft Condensed Matter Physics in Molecular and Cell Biology*, volume 59, page 97–122. Taylor and Francis, Jan 2006.
- <sup>7</sup>Kerensa Broersen, Mireille Weijers, Jolan de Groot, Rob. J. Hamer, and de Jongh. Effect of protein charge on the generation of aggregation-prone conformers. *Biomacromolecules*, 8(5):1648–1656, May 2007.
- <sup>8</sup>Huan-Xiang Zhou and Xiaodong Pang. Electrostatic interactions in protein structure, folding, binding, and condensation. *Chemical Reviews*, 118(4):1691–1741, Feb 2018.
- <sup>9</sup>Martin J. Fossat and Rohit V. Pappu. q-canonical Monte Carlo sampling for modeling the linkage between charge regulation and conformational equilibria of peptides. *The Journal of Physical Chemistry B*, 123(32):6952–6967, Aug 2019.
- <sup>10</sup>Alexey G Murzin. Metamorphic proteins. *Science*, 2008.
- <sup>11</sup>Allen K Kim and Lauren L Porter. Functional and regulatory roles of fold-switching proteins. *Structure*, 29(1):6–14, 2021.
- <sup>12</sup>Sergey V Solomatin, Max Greenfeld, Steven Chu, and Daniel Herschlag. Multiple native states reveal persistent ruggedness of an RNA folding landscape. *Nature*, 463(7281):681–684, 2010.
- <sup>13</sup>Anders Liljas, Lars Liljas, Goran Lindblom, Poul Nissen, Morten Kjeldgaard, and Miriam-rose Ash. *Textbook of structural biology*, volume 8. World Scientific, 2016.
- <sup>14</sup>George C Shields. *Computational approaches for the prediction of pKa values*. CRC Press, 2019.
- <sup>15</sup>Bianca Sclavi, Michael Sullivan, Mark R Chance, Michael Brenowitz, and Sarah A Woodson. RNA folding at millisecond intervals by synchrotron hydroxyl radical footprinting. *Science*, 279(5358):1940–1943, 1998.
- <sup>16</sup>Niels Fischer, Andrey L Konevga, Wolfgang Wintermeyer, Marina V Rodnina, and Holger Stark. Ribosome dynamics and tRNA movement by time-resolved electron cryomicroscopy. *Nature*, 466(7304):329–333, 2010.
- <sup>17</sup>Bruce Jon Compton. Electrophoretic mobility modeling of proteins in free zone capillary electrophoresis and its application to monoclonal antibody microheterogeneity analysis. *Journal of Chromatography A*, 559(1):357–366, Oct 1991.
- <sup>18</sup>Russell S. Negin and Jeffrey D. Carbeck. Determination of effective protein charge by capillary electrophoresis: Effects of charge regulation in the analysis of charge ladders. *Journal of the American Chemical Society*, 72(12):2911–2916, Mar 2002.
- <sup>19</sup>Joshua R. Laber, Barton J. Dear, Matheus L. Martins, Devin E. Jackson, Andrea DiVenere, Jimmy D. Gollihar, Andrew D. Ellington, Thomas M. Truskett, Keith P. Johnston, and Jennifer A. Maynard. Charge shielding prevents aggregation of supercharged GFP variants at high protein concentration. *Molecular Pharmaceutics*, 14(10):3269–3280, Oct 2017.
- <sup>20</sup>Xiao-Hong Nancy Xu and Edward S. Yeung. Electrophoresis of macromolecules in solution detected by electrophoresis-NMR. *Science*, 195(5383):1650–1653, Sep 1998.
- <sup>21</sup>Calin Plesa, Stefan W Kowalczyk, Ruben Zinsmeister, Alexander Y Grosberg, Yitzhak Rabin, and Cees Dekker. Fast translocation of proteins through solid state nanopores. *Nano letters*, 13(2):658–663, 2013.
- <sup>22</sup>Kevin J Freedman, Maik Jürgens, Anmiv Prabhu, Chi Won Ahn, Per Jemth, Joshua B Edelman, and Min Jun Kim. Chemical, thermal, and electric field induced unfolding of single protein molecules studied using nanopores. *Analytical chemistry*, 83(13):5137–5144, 2011.
- <sup>23</sup>Madhavi Krishnan, Nassireddin Mojarad, Philipp Kukura, and Vahid Sandoghdar. Geometry-induced electrostatic trapping of nanometric objects in a fluid. *Nature*, 467(7316):692–695, 2010.
- <sup>24</sup>Francesca Ruggeri, Franziska Zosel, Natalie Mutter, Mirosława Różycka, Magdalena Wojtas, Andrzej Ożyhar, Benjamin Schuler, and Madhavi Krishnan. Single-molecule electrometry. *Nature nanotechnology*, 12(5):488–495, 2017.
- <sup>25</sup>Carlos Macias-Romero, Igor Nahalka, Halil I Okur, and Sylvie Roke. Optical imaging of surface chemistry and dynamics in confinement. *Science*, 357(6353):784–788, 2017.
- <sup>26</sup>Akemi M Darlington and Julianne M Gibbs-Davis. Bimodal or trimodal? the influence of starting pH on site identity and distribution at the low salt aqueous/silica interface. *The Journal of Physical Chemistry C*, 119(29):16560–16567, 2015.
- <sup>27</sup>Sven H Behrens and David G Grier. The charge of glass and silica surfaces. *The Journal of Chemical Physics*, 115(14):6716–6721, 2001.
- <sup>28</sup>Dan Lis, Ellen HG Backus, Johannes Hunger, Sapun H Parekh, and Mischa Bonn. Liquid flow along a solid surface reversibly alters interfacial chemistry. *Science*, 344(6188):1138–1142, 2014.
- <sup>29</sup>Michael S. Bello, Roberta Rezzonico, and Pier Giorgio Righetti. Use of Taylor-Aris dispersion for measurement of a solute diffusion coefficient in thin capillaries. *Science*, 266(5186):773–776, Nov 1994.
- <sup>30</sup>Geoffrey Ingram Taylor. Dispersion of soluble matter in solvent flowing slowly through a tube. *Proceedings of the Royal Society London A*, 219(1137):186–203, 1953.
- <sup>31</sup>Rutherford Aris. On the dispersion of a solute in a fluid flowing through a tube. *Proceedings of the Royal Society London A*, 235(1200):67–77, 1956.
- <sup>32</sup>R. Aris and Geoffrey Ingram Taylor. On the dispersion of a solute in a fluid flowing through a tube. *Proceedings of the Royal Society of London. Series A. Mathematical and Physical Sciences*, 235(1200):67–77, Apr 1956.
- <sup>33</sup>Anthony L Garcia, Linnea K Ista, Dimitar N Petsev, Michael J O'Brien, Paul Bisong, Andrea A Mammoli, Steven RJ Brueck, and Gabriel P López. Electrokinetic molecular separation in nanoscale fluidic channels. *Lab on a Chip*, 5(11):1271–1276, 2005.
- <sup>34</sup>Sumita Pennathur and Juan G Santiago. Electrokinetic transport in nanochannels. 2. Experiments. *Analytical chemistry*, 77(21):6782–6789, 2005.
- <sup>35</sup>Ute Pyell, Alaa H Jalil, Christian Pfeiffer, Beatriz Pelaz, and Wolfgang J Parak. Characterization of gold nanoparticles with different hydrophilic coatings via capillary electrophoresis and Taylor dispersion analysis. part i: Determination of the zeta potential employing a modified analytic approximation. *Journal of colloid and interface science*, 450:288–300, 2015.
- <sup>36</sup>Debashis Dutta. Transport of charged samples in fluidic channels with large zeta potentials. *Electrophoresis*, 28(24):4552–4560, 2007.
- <sup>37</sup>Debashis Dutta. Solutal transport in rectangular nanochannels under pressure-driven flow conditions. *Microfluidics and nanofluidics*, 10(3):691–696, 2011.
- <sup>38</sup>Hilding Faxén. Der widerstand gegen die bewegung einer starren kugel in einer zähen flüssigkeit, die zwischen zwei parallelen ebenen wänden

- eingeschlossen ist. *Annalen der Physik*, 373(10):89–119, 1922.
- <sup>39</sup>M Muthukumar. Communication: Charge, diffusion, and mobility of proteins through nanopores. *The Journal of Chemical Physics*, 141(8):081104, 2014.
- <sup>40</sup>Ali Behjatian, Maria Bespalova, Narain Karedla, and Madhavi Krishnan. Electroviscous effect for a confined nanosphere in solution. *Physical Review E*, 102(4):042607, 2020.
- <sup>41</sup>Henrik Bruus. *Theoretical microfluidics*, volume 18, chapter 3.4.1. Oxford University Press Oxford, 2008.
- <sup>42</sup>CL Henry and VSJ Craig. Measurement of no-slip and slip boundary conditions in confined newtonian fluids using atomic force microscopy. *Physical Chemistry Chemical Physics*, 11(41):9514–9521, 2009.
- <sup>43</sup>Mohamed A Samaha and Mohamed Gad-el Hak. Slippery surfaces: A decade of progress. *Physics of Fluids*, 33(7):071301, 2021.
- <sup>44</sup>Narain Karedla, Jan Christoph Thiele, Ingo Gregor, and Jörg Enderlein. Efficient solver for a special class of convection-diffusion problems. *Physics of Fluids*, 31(2):023606, 2019.
- <sup>45</sup>Jan Christoph Thiele, Ingo Gregor, Narain Karedla, and Jörg Enderlein. Efficient modeling of three-dimensional convection–diffusion problems in stationary flows. *Physics of Fluids*, 32(11):112015, 2020.
- <sup>46</sup>Geoffrey Ingram Taylor. The dispersion of matter in turbulent flow through a pipe. *Proceedings of the Royal Society London A*, 223(1155):446–468, 1954.
- <sup>47</sup>Michael L Parks and Louis A Romero. Taylor-Aris dispersion in high aspect ratio columns of nearly rectangular cross section. *Mathematical and computer modelling*, 46(5-6):699–717, 2007.
- <sup>48</sup>Hong Qian, Michael P Sheetz, and Elliot L Elson. Single particle tracking. analysis of diffusion and flow in two-dimensional systems. *Biophysical Journal*, 60(4):910–921, 1991.
- <sup>49</sup>J Devlin, Dirk Husmeier, and JA Mackenzie. Optimal estimation of drift and diffusion coefficients in the presence of static localization error. *Physical Review E*, 100(2):022134, 2019.
- <sup>50</sup>Per Linse and Bo Jönsson. A monte carlo study of the electrostatic interaction between highly charged aggregates. a test of the cell model applied to micellar systems. *The Journal of Chemical Physics*, 78(6):3167–3176, 1983.
- <sup>51</sup>Luc Belloni. Ionic condensation and charge renormalization in colloidal suspensions. *Colloids and Surfaces A: Physicochemical and Engineering Aspects*, 140(1-3):227–243, 1998.
- <sup>52</sup>Madhavi Krishnan. A simple model for electrical charge in globular macromolecules and linear polyelectrolytes in solution. *The Journal of Chemical Physics*, 146(20):205101, 2017.